Current-Driven Rotating-Kink Mode in a Plasma Column with a Non-Line-Tied Free End

I. Furno,[1,*] T. P. Intrator,[1] D. D. Ryutov,[2] S. Abbate,[1] T. Madziwa-Nussinov,[1] A. Light,[1] L. Dorf,[1] and G. Lapenta[1]

[1]*Los Alamos National Laboratory, Mail Stop E526, Los Alamos, New Mexico 87545, USA*
[2]*Lawrence Livermore National Laboratory, Livermore, California 94551, USA*

(Received 12 March 2006; published 7 July 2006)

First experimental measurements are presented for the kink instability in a linear plasma column which is insulated from an axial boundary by finite sheath resistivity. An instability threshold below the classical Kruskal-Shafranov threshold, axially asymmetric mode structure, and rotation are observed. These are accurately reproduced by a recent kink theory, which includes axial plasma flow and one end of the plasma column that is free to move due to a non-line-tied boundary condition.

DOI: 10.1103/PhysRevLett.97.015002 PACS numbers: 52.35.Py, 52.30.Cv, 52.70.Ds, 52.70.Kz

The current-driven kink instability is a magnetohydrodynamic (MHD) instability which affects current-carrying plasmas in nature and in the laboratory. The kink mode structure and stability condition are strongly dependent on the system geometry and the boundary conditions (BCs). Kruskal [1] and Shafranov [2] (hereafter referred to as KS) considered first the ideal MHD stability of a cylindrical plasma column with magnetic field components $(0, B_\theta, B_z)$ using cylindrical coordinates (r, θ, z). For an infinitely long (equivalent to periodic axial BCs) column, they obtained a linearly unstable helical kink mode of structure $\xi = e^{i(\theta+2\pi z/L)}$ when the plasma current I_p exceeds the Kruskal-Shafranov limit

$$I_{\mathrm{KS}} = (2\pi)^2 a^2 B_z/(\mu_0 L), \tag{1}$$

where a and L are, respectively, the radius and length of the current channel, and ξ is the displacement of the plasma column from the equilibrium position. The KS theory has been quite successful in predicting the behavior of toroidal plasmas for which the periodic BCs yield a proper accounting for the finite length of the system. In linear systems, however, substantial deviations from KS predictions can result from different axial BCs.

The importance of the BCs has long been recognized [3,4] and is of particular relevance to the stability of line-tied flux ropes in space physics (c.f. Ref. [5] and survey Ref. [6]), and astrophysical jets [7]. In recent years, there has been a renewed interest in the stability of a line-tied plasma column in laboratory devices (see Refs. [8–10] and references therein). The kink stability of a plasma column with line-tied ends has been investigated in linear devices, where line-tying is attributed to the presence of highly conducting end plates [11], and in open systems to a local discontinuity for the Alfvén velocity that forms a virtual boundary around the system [12,13].

In this Letter, we experimentally investigate the external kink instability in conditions where one end of the plasma column is line-tied to the plasma source, and the other end is not line-tied and therefore free to slide over the surface of the end plate. The latter BC is a result of plasma sheath resistance that insulates, at least partially, the plasma from the end plate. Compared to the line-tied case, we find significant differences in the kink mode structure and lower critical current for the onset of the kink. The axial flow velocity, the direction of the axial magnetic field, and the rotation frequency of the kink mode are all correlated. The experimental results agree with the predictions from a recent theory of the external kink instability for a slender plasma column [14].

The experiments are conducted in the reconnection scaling experiment (RSX) which uses electrostatic plasma guns to generate the plasma [15]. Figure 1 shows the experimental setup with a view of the plasma gun located at $z = 0$ and radially inserted into the center of the RSX cylindrical vacuum vessel (4 m length and radius $r_{\mathrm{wall}} = 0.2$ m). A hydrogen arc plasma is ejected to form a cylindrical plasma column in a constant, uniform, axial magnetic field of $B_z = 0.012$ T generated by external coils, Figure 1 (5). Electron density and temperature have Gaussian profiles with half-maximum radius $r_0 \approx 2$ cm such that $r_0 \ll r_{\mathrm{wall}}$. Central electron density and temperature are $n_{e0} = 1\text{–}3 \times 10^{19}$ m^{-3} and $T_{e0} = 5\text{–}14$ eV, and axially decrease away from the gun. The axial velocity

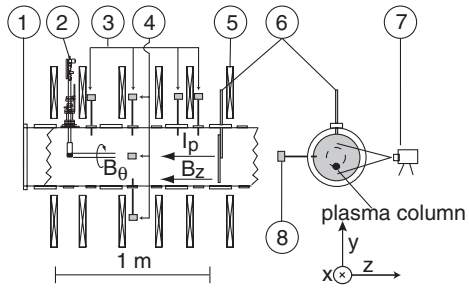

FIG. 1. Experimental setup with diagnostics and coordinate system. (1) Vacuum vessel; (2) plasma gun; magnetic probes in (3) an axial array and (4) an azimuthal array; (5) external coils; (6) external anode. On the right, an axial cut near the external anode. The fast camera (7) is located at the midplane and views the plasma column along the x direction. The bidimensional magnetic probe (8) measures $(\delta B_x, \delta B_y)$ at the edge. Also schematically shown is the plasma column whose end rotates at the external anode.

 © 2006 The American Physical Society

$v_z \approx 3$–5×10^4 ms^{-1} of the plasma has been estimated by solving the momentum balance equations for dominantly axial flow constrained by experimentally measured axial gradients in pressure and density. A current is driven in the plasma by negatively biasing the gun with respect to an external anode (0.05 m^2 stainless steel plate) which is electrically isolated from the vacuum vessel. The external anode can be positioned at different axial locations $z =$ 0.3–3 m allowing the length L of the current-carrying plasma column to be varied.

The MHD activity is monitored by two arrays of magnetic probes that include a total of seven coils inserted in the vacuum vessel at $r_p = 0.15$ m to measure the azimuthal magnetic field B_θ. In the axial array, Fig. 1 (3), four magnetic probes are positioned at $\theta = \pi/2$ (top of the vessel) and axially located at $z = 0.14$, 0.48, 0.62 and 0.76 m. In the azimuthal array, Fig. 1 (4), the four magnetic probes are located at $z = 0.48$ m and azimuthally equispaced by $\pi/2$. One magnetic probe is shared by the two arrays. Signals are digitized at 20 MHz.

In Fig. 2(a), the time evolution of the plasma current measured at the external anode is shown for a discharge with $L = 0.92$ m. The plasma current starts at $t = 0$ when the bias is turned on (arc discharge starts at $t = -1$ ms) and after ≈ 150 μs reaches a stationary phase which lasts for ≈ 1.4 ms. The total plasma current $I_p \approx 320$ A during the stationary phase is determined by the bias voltage and can be varied in the range $I_p = 0.05$–1 kA. Figure 2(b) shows the time evolution of B_θ as measured by the magnetic probe located at $z = 0.48$ m, $\theta = \pi/2$.

For an expanded time window during the stationary phase, measurements of the perturbed azimuthal magnetic field δB_θ from the azimuthal, Fig. 2(c), and the axial, Fig. 2(d), arrays of probes show oscillations with $m = 1$ azimuthal periodicity at the frequency $f \approx 50$ kHz. These oscillations are observed when I_p exceeds a current threshold I_{crit} (see below), but are not detectable for $I_p < I_{\text{crit}}$. The observed instability growth time $\tau_G \approx 4$ μs is of the order of the axial Alfvén time.

The $m = 1$ azimuthal structure is consistent with a plasma column rotating as a rigid body at frequency f. The phase of the signals from the axial array increases linearly along the z direction, Fig. 2(d), indicating a rotating helical current channel. The kinked deformation is a right (left) handed helix if $J_z \cdot B_z > 0$ (< 0), as expected from a paramagnetic kink [12]. The direction of rotation reverses when reversing the external magnetic field B_z. In both cases, the mode rotation is such that the helix always *screws* into the external anode. Both the rotation frequency and the average amplitude of the δB_θ oscillations at the dominant frequency during the stationary phase scale linearly with I_p as shown in Figs. 3(b) and 3(a) where the plasma current is varied in the range 86 A $< I_p <$ 190 A for a plasma column length $L = 0.92$ m. The plasma current corresponding to the limit $\delta B_\theta \to 0$ corresponds to the kink stability threshold which for these data is $I_{\text{crit}} = 70 \pm 7$ A. The rotation frequency at the stability threshold is $f_{\text{crit}} = 28 \pm 3.5$ kHz, Fig. 3(b).

Figure 3(c) shows the axial structure of the $m = 1$ mode close to criticality for $I_p \approx 1.2 \times I_{\text{crit}}$. While a line-tied BC holds at the gun, the large amplitude of the mode at $z \geq 0.76$ m can only occur if the plasma slides over the external anode and is therefore not line-tied. This is confirmed by images of the plasma column at the external anode as shown in Fig. 4. H_α emission is imaged with a Cooke DiCam Pro intensified camera [16] that views the external anode edge perpendicularly to the z axis, Fig. 1 (7). In Figs. 4(a) and 4(b), two fast-gated (200 ns gate $\ll$ Alfvén time) images show, respectively, the plasma column in the equilibrium position and at the maximum displacement ζ_L during the rotation.

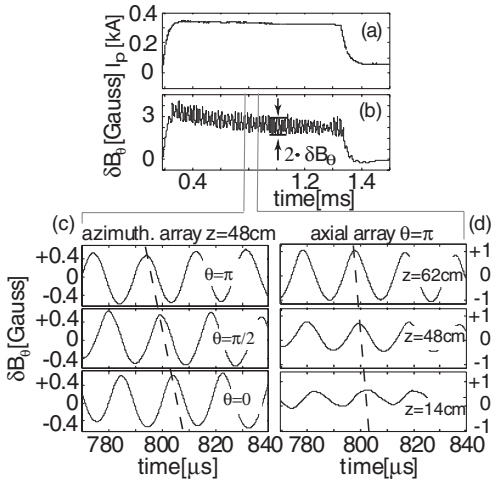

FIG. 2. Time histories of (a) the plasma current; (b) azimuthal magnetic field B_θ (at $z = 0.48$ m, $\theta = \pi/2$, $r = 0.15$ m). Expanded view of the temporal evolution of δB_θ from azimuthal (c) and axial (d) arrays of magnetic probes during the stationary phase of the discharge.

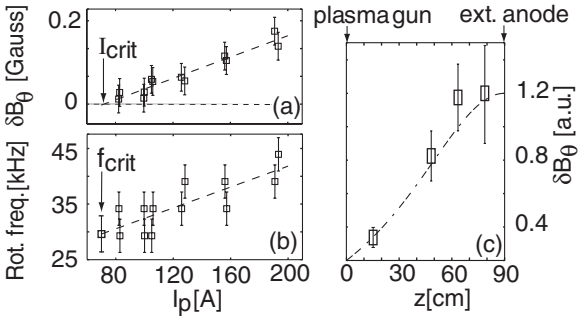

FIG. 3. (a) Amplitude of the perturbed azimuthal magnetic field, δB_θ, and (b) rotation frequency of the mode during the stationary phase as a function of I_p. (c) Axial structure of δB_θ close to the instability threshold for $I_p/I_{\text{crit}} \approx 1.2$ showing non-line-tied BC at the external anode. The dot-dashed line shows the structure of δB_θ as predicted from theory.

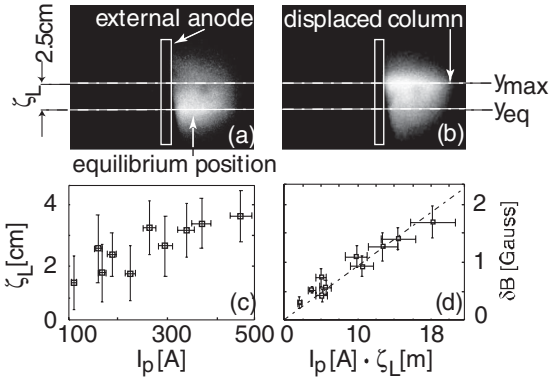

FIG. 4. Optical and magnetic measurements near the external anode demonstrate PNLT BC. As the plasma gun shoots from right to left, a fast-gated image of visible emission shows (a) the equilibrium, y_{eq}, and (b) the displaced, y_{max}, position of the plasma during the rotation. (c) Measured optical displacement $\zeta_L = |y_{max} - y_{eq}|$ for different I_p values. (d) Magnetic field perturbation $\delta B = (\delta B_x^2 + \delta B_y^2)^{1/2}$ versus $I_p \zeta_L$ compared with predictions from Eq. (2) (dashed line). ζ_L and $\delta B_{x,y}$ are measured 0.01 m in front of the external anode.

The observed sliding of the plasma column over the external anode surface is not consistent with a line-tied BC, which might be presumed at the external anode for time scales less than its 100–200 μs resistive diffusion time. Deviations from line-tying may appear if the plasma is insulated from the external anode by a finite plasma sheath resistance. The degree of insulation is measured by the ratio κ of the Alfvén transit to inductive decay times of the current [14]. We estimate $\kappa \approx 15$ from the formula $\kappa \approx (c_s/v_z)[c/(a\omega_{pi})]^2\beta_e^{1/2}$ where $c_s = (T_e/m_i)^{1/2}$, $\beta_e = 2\mu_0 n_e T_e/B_z^2$ and ω_{pi} is the plasma frequency (derivation in Ref. [14]) for typical plasma parameters $a \approx 2$ cm, $T_e \approx 10$ eV, $n_e \approx 10^{19}$ m^{-3}, $v_z/c_s \approx 1$. For the present experiments, we conclude that $\kappa \gg 1$ and the plasma is insulated from the conducting boundary by finite sheath resistance. Ryutov and coauthors [14] have shown that for $\kappa \gg 1$ the BC can be formulated as $[\partial\zeta/\partial z + i(k_0/2)\zeta]|_{z=L} = 0$ where $k_0 = B_\theta/(aB_z) = \mu_0 I_p/(2\pi a^2 B_z)$ with Cartesian complex displacement $\zeta = \xi_x(z, t) + i\xi_y(z, t)$. In the following, we will refer to this condition as to *perfect nonline-tying* (PNLT) BC and we will show that it holds at the external anode, after using an equivalent condition that can be directly compared with experimental data.

With a thin plasma column approximation ($a \ll r_{wall}$, L) and assuming that $r = 0$ is the equilibrium position, the Cartesian components of the perturbed magnetic field at $r = r_p \gg a$ can be expressed as $\delta B_{x,y} = (a^2/r_p^2)B_z(\partial\xi_{x,y}/\partial z \pm k_0\xi_{y,x})$. Using the PNLT condition, in the vicinity of the external anode the perturbed magnetic field can be expressed as

$$\delta B = (\delta B_x^2 + \delta B_y^2)^{1/2} = I_p \zeta_L (3\mu_0)/(4\pi r_p^2) \qquad (2)$$

where $\zeta_L = [\xi_x(L, t)^2 + \xi_y(L, t)^2]^{1/2}$.

We use magnetic measurements combined with images near the external anode to test Eq. (2), equivalent to the PNLT condition. Images such as those in Figs. 4(a) and 4(b) determine the maximum displacement y_{max} and equilibrium y_{eq} positions of emissivity along a line parallel to the external anode surface and axially spaced 0.01 m in front of it. The image in Fig. 4(b) is synchronized to a magnetic probe at the same axial location but azimuthally separated by $\pi/2$ to provide the position of maximum column displacement. In Fig. 4(c), the displacement $\zeta_L = |y_{max} - y_{eq}|$ is shown for a series of discharges with 100 A $< I_p <$ 500 A. In Fig. 4(d), the magnetic perturbations (δB_x, δB_y) are measured at $r_p = 0.17$ m and 1 cm in front of the external anode using a bidimensional magnetic probe. In Fig. 4(d), the experimental data show excellent agreement with the PNLT predicted scaling in Eq. (2) (shown as a dashed line). We therefore conclude that the PNLT BC applies to the external anode.

For a PNLT BC at $z = L$ and with axial plasma flow velocity v_z, the eigensolution for the MHD equation of motion [Eq. (57) in Ref. [14]] is $\zeta = C(e^{ik^+ z} - e^{ik^- z})e^{i\theta - i\omega t}$ with axial wave numbers $k^\pm = \pm(\pi/2L) \times [1 \mp (1 - M^2)^{1/2}]$ where $M = v_z/(\sqrt{2}\bar{v}_A)$ is the Alfvén Mach number, and $\bar{v}_A$ is calculated using the average density $\bar{n}_e = (2/a^2)\int_0^a n_e(r) r dr$. In Fig. 3(c), the axial structure of δB_θ from experimental data for $I_p \approx 1.2 \times I_{crit}$ (squares) and from the theoretical eigensolution (dot-dashed line) are compared. The good agreement suggests a robustness of the eigensolution for slightly supercritical regimes. The total axial phase shift at criticality (not shown here) is also consistent within the experimental uncertainties with the expected eigensolution for Mach numbers in the range $M = 0.25$–0.4.

The critical current in this case is

$$I_{crit} = \frac{1}{2}\frac{(2\pi a)^2 B_z}{\mu_0 L}(1 - M^2)^{1/2} \equiv \frac{I_{KS}}{2}(1 - M^2)^{1/2}, \qquad (3)$$

showing that the kink mode is unstable at half the KS current for vanishing flow and smaller currents when flow exists. The eigenfrequency ω at the criticality has a finite real component

$$\mathrm{Re}\,(\omega) = -\frac{\sqrt{2}\pi\bar{v}_A}{L} M(1 - M^2)^{1/2}. \qquad (4)$$

The perturbed plasma column rotates at frequency $\mathrm{Re}(\omega) = 2\pi f$, constant along the column. The rotation is driven by axial plasma flow from the gun to the external anode along the helically perturbed column as well as a Doppler shifted $k^\pm \cdot v_z$, such that the helix always *screws* into the external anode, consistently with the experimental observations.

To investigate the applicability of Eqs. (3) and (4), Fig. 5(a) shows the critical current and 5(b) shows the rotation frequency at the criticality as a function of the

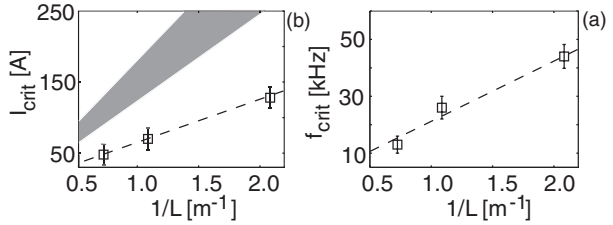

FIG. 5. For three different column lengths ($L = 0.48$, 0.92, 1.38 m): (a) critical current I_{crit} (b) rotation frequency at the criticality f_{crit} as a function of the inverse column length $1/L$. The gray region indicates predictions from KS theory. Dotted lines show linear fits.

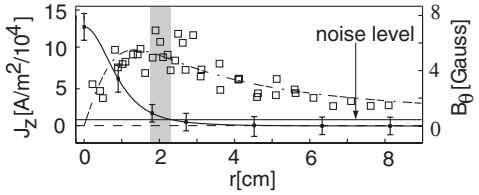

FIG. 6. Radial profile of current density (solid line) from measured azimuthal magnetic field (squares) at the criticality. The vertical gray region indicates the error bounded estimate of a at the edge of the current channel.

inverse column length $1/L$ which is in agreement with a predicted linear scaling.

The system comprising Eqs. (3) and (4) provides a theoretical relationship between I_{crit}, f_{crit}, a, M and the average plasma density (or Alfvén speed). This was solved using experimental measurements of the electron density profile at criticality together with deduced scalings $I_{crit} = 59/L$ [A] and $f_{crit} = 2.4 \times 10^4/L$ [Hz] from the data in Fig. 5. We obtained a radius $a = 2 \pm 0.2$ cm which is in agreement with the experiment (see Fig. 6) and Mach number $M = 0.25$–0.4. The corresponding axial flow velocity $v_z \approx 3 - 4.8 \times 10^4$ ms^{-1} is also consistent with our independent estimate. In Fig. 5, predictions from KS theory using the computed a are compared to the experimental data.

For the external kink, the radius a is expected at the position where conductivity, magnetic diffusion time, and axial-vector current density $J_z(r)$ are negligibly small. This is tested using profile measurements at the criticality. Figure 6 shows a Bennet profile least-squares fit of $J_z(r)$ at the instability threshold, as obtained from azimuthal magnetic field measurements at $z = 0.48$ m for $L = 0.92$ m. The previously determined radius $a = 2 \pm 0.2$ cm is located at the edge of the profile where $J_z(a) \approx 0.05 \times J_z(0)$. Similar conclusions follow from the magnetic diffusivity, derived from the measured electron temperature profile and the observed instability growth time τ_G.

It should be emphasized here that the measurements in this Letter only characterize the global structure of the external kink mode. Although some of the observations (e.g., axial structure and rotation frequency of the mode) show some resemblance with measurements of internal drift-Alfvén waves in finite-β plasmas with axial current [17], additional internal measurements will be needed to investigate the presence of these waves in our experiment.

In summary, we have presented first experimental results for the current-driven kink instability in a plasma column with one free end that is not line-tied to its boundary due to a finite sheath resistance. Mode structure and instability threshold are significantly different from predictions from the Kruskal-Shafranov theory and are accurately reproduced by a recently developed kink theory. The finite rotation of the mode, which is also observed in other laboratory devices [11,13], is due to the plasma flow along the helically kinked plasma column.

Though not addressed here, the effect of a non-line-tied end should be important for the relaxing kinked plasma column. A destabilizing $\vec{J}_\theta \times \vec{B}_z$ force coexists with a stabilizing curvature force due to axial field line bending. The free end allows shifts with reduced curvature and restoring force possibly resulting in a helical saturated state of larger displacement than the line-tied case. Numerical simulations are being implemented for the nonlinear evolution of the kink mode.

Support by Los Alamos Laboratory Directed Research and Development—Exploratory Research program, and Associazione Sviluppo Piemonte for S. A. is gratefully acknowledged.

*Current Address: CRPP, Association EURATOM-Confédération Suisse, EPFL, Lausanne, Switzerland. Email address: ivo.furno@epfl.ch

[1] M. Kruskal and J. L. Tuck, Proc. R. Soc. A **245**, 222 (1958).
[2] V. D. Shafranov, At. Energ. **5**, 38 (1956).
[3] L. S. Solov'ev, Sov. At. Energy **30**, 14 (1971).
[4] M. A. Raadu, Sol. Phys. **22**, 425 (1972).
[5] H. Baty, Astron. Astrophys. **318**, 621 (1997).
[6] A. W. Hood, Plasma Phys. Controlled Fusion **34**, 411 (1992).
[7] D. L. Meier, S. Koide, and Y. Uchida, Science **291**, 84 (2001).
[8] I. M. Lanskii and A. I. Shchetnikov, Sov. J. Plasma Phys. **16**, 322 (1990).
[9] D. D. Ryutov, R. H. Cohen, and L. D. Pearlstein, Phys. Plasmas **11**, 4740 (2004).
[10] C. C. Hegna, Phys. Plasmas **11**, 4230 (2004).
[11] W. F. Bergerson *et al.*, Phys. Rev. Lett. **96**, 015004 (2006).
[12] S. C. Hsu and P. M. Bellan, Phys. Rev. Lett. **90**, 215002 (2003).
[13] M. Zuin *et al.*, Phys. Rev. Lett. **92**, 225003 (2004).
[14] D. D. Ryutov *et al.*, Phys. Plasmas **13**, 032105 (2006).
[15] I. Furno *et al.*, Rev. Sci. Instrum. **74**, 2324 (2003).
[16] E. Hemsing, I. Furno, and T. Intrator, IEEE Trans. Plasma Sci. **33**, 448 (2005).
[17] J. T. Tang *et al.*, Phys. Rev. Lett. **34**, 70 (1975); J. T. Tang and N. C. Luhman, Jr., Phys. Fluids **19**, 1935 (1976).